Earth and Planetary Science Letters 361 (2013) 16–25

Contents lists available at SciVerse ScienceDirect

Earth and Planetary Science Letters

journal homepage: www.elsevier.com/locate/epsl

Timing of the last glaciation and subsequent deglaciation in the Ruby Mountains, Great Basin, USA

Benjamin J.C. Laabs [a,*], Jeffrey S. Munroe [b], Laura C. Best [a,1], Marc W. Caffee [c]

[a] Department of Geological Sciences, SUNY Geneseo, USA
[b] Department of Geology, Middlebury College, USA
[c] Department of Physics, PRIME Lab, Purdue University, USA

ARTICLE INFO

Article history:
Received 13 June 2012
Received in revised form
2 November 2012
Accepted 9 November 2012
Editor: J. Lynch-Stieglitz

Keywords:
Great Basin
mountain glaciation
cosmogenic surface-exposure dating
Ruby Mountains
Nevada

ABSTRACT

The timing of the last Pleistocene glaciation in western North America is becoming increasingly well understood, largely due to improved methods of obtaining numerical ages of glacial deposits and landforms. Among these, cosmogenic radionuclide surface-exposure dating has been widely applied to moraines of mountain glaciers, providing the framework for understanding terrestrial climate change during and since the last glaciation in western North America. During the Late Pleistocene, the Great Basin of the western United States hosted numerous mountain glaciers, the deposits of which can provide valuable records of past climate changes if their ages can be precisely determined. In this study, twenty-nine cosmogenic radionuclide ^{10}Be surface-exposure ages from a suite of moraines in Seitz Canyon, western Ruby Mountains, limit the timing of the last glacial episode in the interior Great Basin, known as the Angel Lake Glaciation. Results indicate that deposition of a terminal moraine and two recessional moraines began just prior to ~20.5 ka and continued until ~20.0 ka. Retreat from the next younger recessional moraine began at ~17.2 ka, and final deglaciation began at ~14.8 ka. These ages are broadly consistent with cosmogenic surface-exposure ages from the eastern Sierra Nevada and the western Wasatch Mountains, in the western and eastern extremes of the Great Basin respectively. Furthermore, these ages suggest that the valley glacier in Seitz Canyon was at or near its maximum extent before and during the hydrologic maxima of Pleistocene lakes in the Great Basin, supporting previous suggestions that a cool and wet climate persisted in this region during the early part of the last glacial–interglacial transition.

1. Introduction

The surficial geology and geomorphology of the Great Basin, a broad area of internal drainage in the southwestern United States, have long been recognized as key records of environmental changes during the late Quaternary (e.g., Gilbert, 1890; Blackwelder, 1931; Sharp, 1938). Numerous studies aimed at understanding paleoenvironmental changes in this region have focused on deposits of large Pleistocene lakes (e.g., Benson and Thompson, 1987) and on records of glaciation in mountain ranges that border the Great Basin (e.g., the Sierra Nevada in California, and the Wasatch and Uinta Mountains in Utah, Fig. 1). The record of Pleistocene glaciations in the interior mountains of the Great Basin (Blackwelder, 1931; Osborn and Bevis, 2001) is also valuable for understanding paleoenvironmental changes but has been generally overlooked.

The glacial geology of the Great Basin features deposits of former mountain glaciers (Blackwelder, 1931, 1934) in more than forty individual ranges (Osborn and Bevis, 2001). The Ruby and East Humboldt Mountains (Fig. 1) hosted the largest system of mountain glaciers of all the interior ranges (Munroe and Laabs, 2011). Here, the glacial record in these mountains is interpreted as representing two major glacial episodes, the Lamoille (penultimate) Glaciation, named for a broad, hummocky terminal moraine complex at the mouth of Lamoille Canyon in the western Ruby Mountains, and the Angel Lake (last) Glaciation, named for nearly continuous lateral and terminal moraines in the valley that hosts Angel Lake in the northeastern East Humboldt Mountains (Sharp, 1938). Osborn and Bevis (2001) summarize the record of these two glaciations throughout the Great Basin and emphasize the exceptional preservation of the glacial record in the Ruby and East Humboldt Mountains in particular. Reconstructions based on glacial-geomorphic evidence indicate that, during the Angel Lake Glaciation, these mountains hosted more than 130 discrete valley glaciers within a north–south distance of 150 km (Osborn and Bevis, 2001; Laabs et al., 2011; Munroe and Laabs, 2011). Throughout

* Corresponding author. Tel.: +1 585 245 5305.
E-mail address: laabs@geneseo.edu (B.J.C. Laabs).
[1] Current address: Department of Geology, SUNY Buffalo, USA.

0012-821X/$ - see front matter © 2012 Elsevier B.V. All rights reserved.
http://dx.doi.org/10.1016/j.epsl.2012.11.018

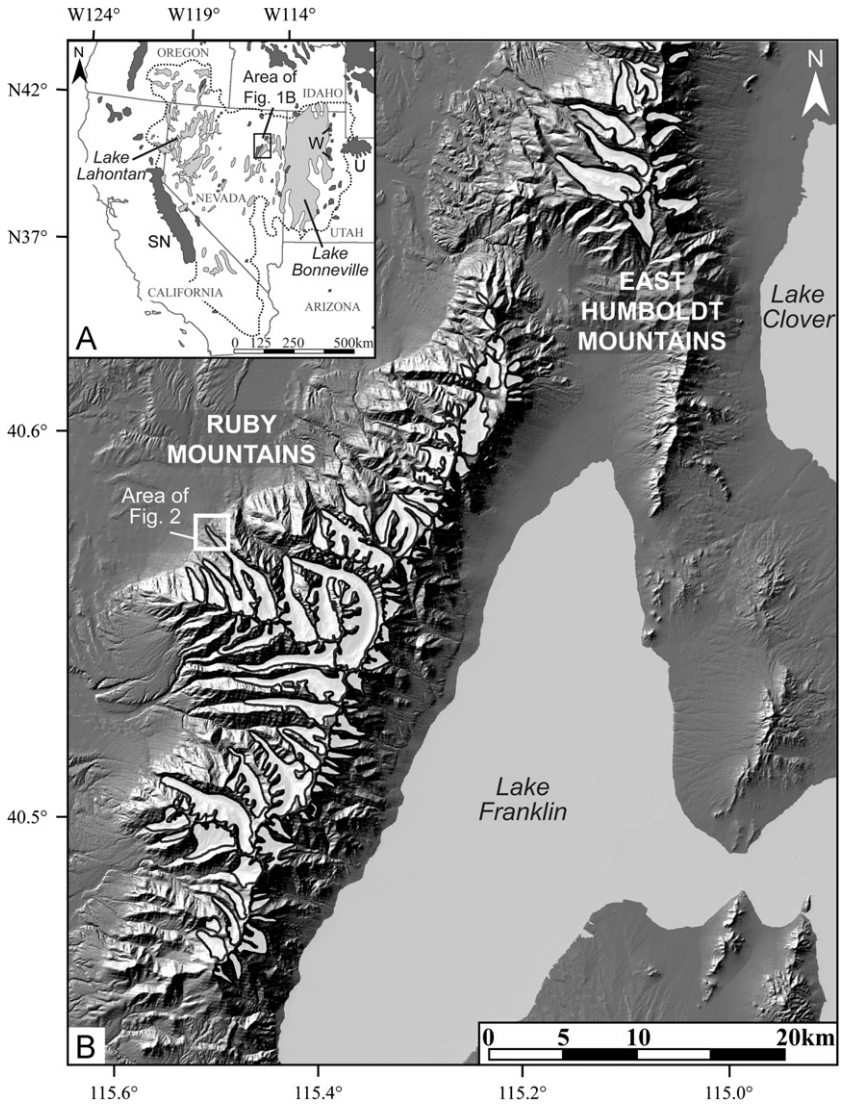

Fig. 1. (A) Map of a portion of the southwestern United States. Dashed line indicates the Great Basin region. Pleistocene mountain glacier systems (modified from Porter et al., 1983) and paleolakes (from Reheis, 1999) are shown in dark and light gray, respectively. SN=Sierra Nevada, U=Uinta Mountains and W=Wasatch Mountains. (B) Shaded-relief map of the Ruby and East Humboldt Mountains and adjacent valleys. Extents of valley glaciers for the Angel Lake Glaciation are shown in white with black outline. Lakes Franklin and Clover are Pleistocene lakes that were adjacent to the mountains.

these mountains, moraine sequences suggest a dynamic history of ice advance and retreat during the Angel Lake Glaciation.

Given its excellent preservation, the glacial record of the Ruby and East Humboldt Mountains offers great potential for understanding the magnitude and timing of the Angel Lake Glaciation. However, in the context of developing a chronology of glaciation, these mountains have received considerably less attention than the Sierra Nevada (e.g., Burke and Birkeland, 1979; Phillips et al., 1990; Phillips et al., 2009; Rood et al., 2011) and the Wasatch and Uinta Mountains (Madsen and Currey, 1979; Munroe et al., 2006; Laabs et al., 2009, 2011), which are nearer to major population centers. Developing a glacial chronology for the interior Great Basin is important for several reasons. First, the Ruby Mountains are centrally located among well-dated Pleistocene glacial locales in the interior of the western US, including the Sierra Nevada (e.g., Phillips et al., 1990, 2009), the Northern and Middle Rocky Mountains (e.g., Gosse et al., 1995; Licciardi and Pierce, 2008), and the Colorado Plateau (Marchetti et al., 2005). Given the apparent variability in the timing of mountain glacier maxima among these areas (Thackray, 2008), data from the Great Basin can fill a significant gap in the understanding of mountain glaciation and may help identify the causes of this variability. Additionally, the Ruby Mountains lie between areas occupied by the two largest Pleistocene lakes in the Great Basin, Bonneville and Lahontan (Fig. 1A), both of which have well-dated hydrographs based on radiocarbon dating of lacustrine deposits (e.g., Oviatt, 1997; Benson et al., in press). Setting clear limits on the relative timing of glaciation in the mountains and of lake highstands on valley floors provides a framework for understanding (1) the hydrologic relationship of mountain glaciers and lakes, (2) differences in the sensitivity of mountain glaciers and lakes to climate changes during the last glaciation, and (3) the timing of regional-scale climate changes that affected lake highstands and glacier maxima. Finally, given the relatively small size (~1–15 km in length) of the valley glaciers that occupied the Ruby Mountains, these glaciers were undoubtedly sensitive to both millennial- and centennial-scale climate changes during the Angel Lake Glaciation, which may be reflected in their moraine records.

In this paper, a suite of cosmogenic radionuclide ^{10}Be surface-exposure ages (hereafter referred to as "surface-exposure ages") from one of the best-preserved moraine sequences in the Ruby Mountains provides the first direct numerical age limits on glacial

deposits in the interior Great Basin. These surface-exposure ages limit the timing of the Angel Lake Glaciation and the subsequent deglaciation. These results are then compared to previously reported ages of moraines from the extreme western and eastern margins of the Great Basin to reveal regional patterns in the timing of the last Pleistocene glaciation.

2. Setting

The Ruby Mountains are one of several ranges in northern Nevada that typify the distinct Basin-and-Range topography (Fig. 1), rising more than 2 km above the adjacent valley floors (Howard et al., 1979; Satarugsa and Johnson, 2000). In general, west-flowing drainages have gentler slopes and greater lengths, likely reflecting the asymmetric pattern of uplift along range-bounding normal faults (Howard et al., 1979). The largest valley glaciers in the range (with surface areas as great as 20 km^2) occupied west-flowing drainages near the central-west portion of the range, where summit elevations are as high as 3471 m (Ruby Dome). Throughout the Ruby Mountains, spectacular alpine glacial geomorphology is the clearest evidence of Pleistocene glaciations, along with terminal moraines that delimit the extents of glaciers during the Lamoille and Angel Lake Glaciations (Munroe and Laabs, 2011). The distribution of terminal moraines indicates that most glaciers were entirely restricted to bedrock valleys, where moraines are somewhat fragmented and obscured due to erosion by hill-slope processes and mountain streams. In some settings, however, ice extended out to the piedmont where terminal moraines are better preserved.

Seitz Canyon features well-preserved terminal moraines, representing the Lamoille and Angel Lake Glaciations (Fig. 2). The Lamoille-age deposits are continuous lateral moraines, featuring triangular facets (with 10–20 m of relief) where they are offset by Pleistocene normal faults at the range front. The Angel Lake-age moraines are nested behind the Lamoille-age moraines and form a multi-crested moraine complex, with some crests separated by distinct outwash fans. All moraine crests feature large erratic boulders (up to 3 m in diameter) of a variety of lithologies derived from the metamorphic core complex that comprises the Ruby Mountains (Satarugsa and Johnson, 2000). Among these, migmatite, pegmatitic granite and gneiss, monzonite and quartzite are dominant. In general, moraines deposited during the Angel Lake Glaciation feature a greater frequency of large boulders on their crests compared to moraines deposited during the Lamoille Glaciation. Additionally, the crests of the Lamoille moraines are broader and are relatively subdued beyond the range front where they are locally buried by outwash deposited during the Angel Lake Glaciation.

3. Methods

Moraines at Seitz Canyon were mapped on 1:24,000 scale topographic maps and checked in the field. A terminal and six recessional moraines identified as Angel Lake-equivalent deposits (Munroe and Laabs, 2011; Fig. 2) were explored to identify erratic boulders suitable for surface-exposure dating. The tallest (>0.75 m) and widest (width $>$ height) boulders composed of quartz-bearing lithologies and featuring broad, horizontal surfaces with glacial polish or minimal evidence of surface erosion were identified as suitable. In some cases, resistant protruding knobs on boulders indicate that some erosion had occurred; erosion rates of $1–3\times10^{-4}$ cm/yr were estimated for these surfaces based on their measured relief. The number of samples collected from each moraine crest was dependent on the availability of suitable boulders, and ranges from two (in just two cases) to eight (Table 1). Samples were collected with a sledgehammer and chisel and had masses ranging from 1 to 4 kg, with smaller masses collected from boulder lithologies with the greatest concentration of quartz.

All samples were prepared at SUNY Geneseo for *in situ* cosmogenic ^{10}Be measurement following methods modified from Kohl and Nishiizumi (1992), Ditchburn and Whitehead (1994), Bierman et al. (2002) and Munroe et al. (2006). Samples were reduced to an approximately uniform thickness of 2–5 cm (except in cases where

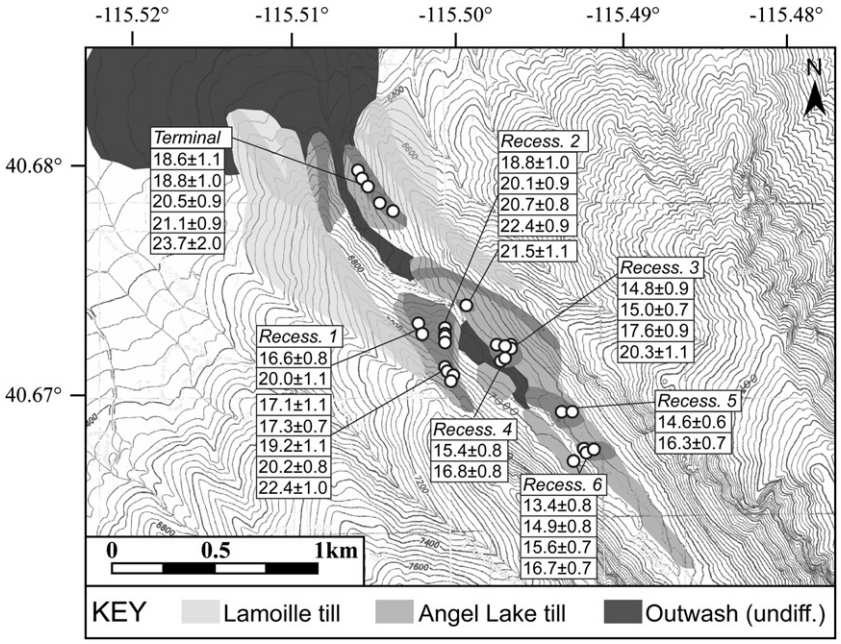

Fig. 2. Topographic map and glacial geology near the mouth of Seitz Canyon, western Ruby Mountains (topographic map based from the USGS 7.5-minute Lamoille and Noon Rock quadrangles). Gray areas indicate mapped till and outwash of the Angel Lake and Lamoille Glaciations; darkened areas within mapped till indicate moraine crests. Moraine names are as follows: "Terminal"=terminal moraine of the Angel Lake Glaciation; "Recess. 1"=outermost recessional moraine of the Angel Lake Glaciation; all other recessional moraines (Recess. 2–6) are progressively younger with distance upvalley. Circles indicate locations of boulders sampled for surface-exposure dating. Surface-exposure ages are given in kyr $\pm 1\sigma$ internal error (see Table 1).

Table 1
^{10}Be data and surface exposure ages for moraines in Seitz Canyon.

Moraine and sample ID	Elevation (m asl)	Latitude (°N)	Longitude (°W)	[^{10}Be] (atoms g SiO_2^{-1})	1σ	Sample thickness[a] (cm)	Erosion rate (cm/yr)	Topographic shielding factor	Lal (1991)/Stone (2000) global constant prod. rate exposure age[b] (ka)	1σ^c internal (kyr)	1σ^d external (kyr)	Lal (1991)/Stone (2000) NENA constant prod. rate exposure age[e] (ka)	1σ^c internal (kyr)	1σ^d external (kyr)
Terminal														
SC-17	1991	40.6805	−115.5059	3.70E+05	1.9E+04	3.0	0.0000	0.99545	**18.8**	**1.0**	**1.9**	**21.5**	**1.1**	**1.5**
SC-18	1998	40.6802	−115.5056	4.13E+05	1.7E+04	4.0	0.0000	0.99479	**21.1**	**0.9**	**2.0**	**24.1**	**1.0**	**1.5**
SC-19	2007	40.6798	−115.5056	3.77E+05	1.6E+04	6.0	0.0003	0.99441	**20.5**	**0.9**	**2.1**	**23.5**	**1.1**	**1.6**
SC-20	2028	40.6791	−115.5048	3.62E+05	2.1E+04	5.5	0.0001	0.99645	**18.6**	**1.1**	**2.0**	**21.3**	**1.3**	**1.6**
SC-21	2040	40.6787	−115.5041	4.76E+05	4.0E+04	4.0	0.0000	0.99414	**23.7**	**2.0**	**2.9**	**27.0**	**2.3**	**2.6**
							mean (n=5, χ^2R=2.26[f], 1σ)=**20.5** ± **2.1**			mean (n=5, χ^2R=2.19[f], 1σ)=**23.5** ± **2.3**					
							EWM (n=5, MSWD=2.1[g], 2σ)=**20.1** ± **0.9**			EWM (n=5, MSWD=2.1[g], 2σ)=**23.0** ± **1.1**				
Recessional 1														
SC-1	2173	40.6710	−115.5007	4.60E+05	2.0E+04	5.0	0.0003	0.992	**22.4**	**1.0**	**2.3**	**25.7**	**1.2**	**1.8**
SC-2	2170	40.6711	−115.5008	3.75E+05	1.6E+04	5.5	0.0000	0.992	**17.3**	**0.7**	**1.7**	**19.8**	**0.8**	**1.3**
SC-3	2169	40.6712	−115.5009	3.92E+05	2.1E+04	7.0	0.0003	0.995	**19.2**	**1.1**	**2.1**	**22.0**	**1.3**	**1.7**
SC-4	2169	40.6712	−115.5010	4.33E+05	1.7E+04	3.0	0.0000	0.995	**19.6**	**0.8**	**1.9**	**22.3**	**0.9**	**1.4**
SC-5	2168	40.6713	−115.5011	3.56E+05	2.1E+04	5.0	0.0003	0.995	**17.1**	**1.1**	**1.9**	**19.6**	**1.2**	**1.6**
SC-6	2125	40.6732	−115.5025	3.42E+05	1.6E+04	3.0	0.0003	0.995	**16.6**	**0.8**	**1.7**	**19.0**	**0.9**	**1.3**
SC-7	2119	40.6733	−115.5026	4.09E+05	2.3E+04	4.0	0.0000	0.995	**19.3**	**1.1**	**2.0**	**22.0**	**1.2**	**1.6**
							mean (n=7, χ^2R=4.80, 1σ)=**18.8** ± **2.0**			mean (n=7, χ^2R=4.67, 1σ)=**21.7** ± **2.4**					
							EWM (n=7, MSWD=4.7, 95% conf.)=**18.5** ± **1.8**			EWM (n=7, MSWD=5.0, 95% conf.)=**21.4** ± **2.2**				
Recessional 2														
SC-22	2116	40.6729	−115.5011	4.17E+05	1.7E+04	6.0	0.0000	0.989	**20.1**	**0.8**	**1.9**	**23.0**	**0.9**	**1.5**
SC-23	2113	40.6730	−115.5010	4.49E+05	1.8E+04	5.0	0.0002	0.989	**22.4**	**0.9**	**2.2**	**25.6**	**1.1**	**1.7**
SC-24	2115	40.6729	−115.5011	4.23E+05	1.8E+04	4.0	0.0000	0.989	**20.1**	**0.9**	**2.0**	**22.9**	**1.0**	**1.5**
SC-25	2112	40.6731	−115.5010	3.85E+05	2.1E+04	5.0	0.0001	0.989	**18.8**	**1.0**	**2.0**	**21.4**	**1.2**	**1.6**
SC-26	2104	40.6742	−115.4998	4.22E+05	2.1E+04	5.0	0.0003	0.989	**21.5**	**1.1**	**2.3**	**24.7**	**1.3**	**1.8**
							mean (n=5, χ^2R=2.15, 1σ)=**20.6** ± **1.4**			mean (n=5, χ^2R=2.06, 1σ)=**23.7** ± **1.6**					
							EWM (n=5, MSWD=2.1, 2σ)=**20.6** ± **0.8**			EWM (n=5, MSWD=1.9, 2σ)=**23.6** ± **1.0**				
Recessional 3														
SC-30	2123	40.6724	−115.4971	3.96E+05	2.0E+04	5.0	0.0003	0.981	**20.0**	**1.1**	**2.1**	**22.9**	**1.2**	**1.7**
SC-32	2110	40.6722	−115.4977	3.72E+05	1.9E+04	2.0	0.0000	0.981	**17.6**	**0.9**	**1.8**	**20.0**	**1.0**	**1.4**
SC-33	2112	40.6722	−115.4976	3.16E+05	1.5E+04	3.0	0.0000	0.981	**15.0**	**0.7**	**1.5**	**17.1**	**0.8**	**1.2**
SC-34	2110	40.6723	−115.4978	3.00E+05	1.8E+04	3.0	0.0003	0.981	**14.8**	**0.9**	**1.6**	**17.0**	**1.1**	**1.4**
							mean (n=4, χ^2R=7.02, 1σ)=**16.9** ± **2.5**			mean (n=4, χ^2R=7.07, 1σ)=**19.4** ± **3.0**					
							EWM (n=4, MSWD=6.5, 95% conf.)=**16.3** ± **3.5**			EWMn (n=4, MSWD=7.2, 95% conf.)=**18.8** ± **4.3**				
Recessional 4														
SC-28	2110	40.6716	−115.4975	3.07E+05	1.6E+04	5.0	0.0003	0.985	**15.4**	**0.8**	**1.6**	**17.6**	**1.0**	**1.3**
SC-29	2114	40.6718	−115.4973	3.22E+05	1.4E+04	10.0	0.0003	0.986	**16.8**	**0.8**	**1.7**	**19.3**	**0.9**	**1.3**
							mean (n=2, χ^2R=1.53, 1σ)=**16.1** ± **1.0**			mean (n=2, χ^2R=1.61, 1σ)=**18.4** ± **1.2**					
							EWM (n=2, MSWD=1.5, 2σ)=**16.1** ± **1.1**			EWM (n=2, MSWD=1.6, 2σ)=**18.5** ± **1.3**				
Recessional 5														
SC-38	2140	40.6692	−115.4936	2.81E+05	1.2E+04	12.0	0.0001	0.963	**14.6**	**0.6**	**1.4**	**16.6**	**0.7**	**1.1**
SC-39	2145	40.6691	−115.4940	3.27E+05	1.3E+04	6.0	0.0001	0.951	**16.3**	**0.7**	**1.6**	**18.6**	**0.8**	**1.2**
							mean (n=2, χ^2R=3.48, 1σ)=**15.5** ± **1.2**			mean (n=2, χ^2R=3.60, 1σ)=**17.6** ± **1.4**					
							EWM (n=2, MSWD=3.4, 2σ)=**15.3** ± **0.9**			EWM (n=2, MSWD=3.6, 2σ)=**17.6** ± **1.0**				
Recessional 6														
SC-41	2148	40.6675	−115.4922	3.02E+05	1.6E+04	5.0	0.0001	0.950	**14.9**	**0.8**	**1.5**	**17.0**	**0.9**	**1.2**
SC-42	2144	40.6674	−115.4926	2.69E+05	1.5E+04	7.0	0.0000	0.945	**13.4**	**0.8**	**1.4**	**15.3**	**0.9**	**1.1**
SC-43	2144	40.6675	−115.4928	3.42E+05	1.4E+04	5.5	0.0000	0.953	**16.7**	**0.7**	**1.6**	**19.1**	**0.8**	**1.2**
SC-44	2145	40.6670	−115.4933	3.07E+05	1.3E+04	9.0	0.0000	0.944	**15.6**	**0.7**	**1.5**	**17.8**	**0.8**	**1.1**
							mean (n=4, χ^2R=3.40, 1σ)=**15.2** ± **1.4**			mean (n=4, χ^2R=3.50, 1σ)=**17.3** ± **1.6**					
							EWM (n=4, MSWD=3.4, 95% conf.)=**15.3** ± **2.2**			EWM (n=4, MSWD=3.7, 95% conf.)=**17.4** ± **2.5**				

Note: All samples have a density of 2.7 g/cm^3 and were measured against Beryllium AMS standard Be-01-5-3 (Nishiizumi et al., 2007), which is coded "07KNSTD" in the CRONUS Earth exposure age calculator.

[a] Sample thickness was minimized in all cases except where the quartz concentration in the rock sample was less than 20%.
[b] Computed from spallogenic plus muogenic production rate scaled from the global reference production rate by the CRONUS online exposure-age calculator, version 2.2 (Balco et al., 2008).
[c] Uncertainty of AMS measurement and scaling of the production rate for sample thickness. Uncertainties of measurements during sample preparation, the Be-half life, and the attenuation of secondary cosmic rays are not included.
[d] Uncertainty of AMS measurement and production rate.
[e] Computed from spallogenic plus muogenic production rate scaled from the Northeast North America reference production rate by the CRONUS online exposure-age calculator, version 2.2 (Balco et al., 2008).
[f] For all moraines, this value is computed from the surface exposure ages ± the internal uncertainty.
[g] MSWD=mean square of weighted deviates. Computed from the same expression as χ^2R, but is based on the error-weighted mean instead of the mean of surface exposure ages. EWM=error-weighted mean.

low quartz concentrations made it necessary to retain thicker samples) prior to crushing, milling, and sieving to separate the 425–850-μm grain size fraction. From this fraction, quartz grains were separated from other minerals using a Franz magnetic separator, heavy liquids, and a series of dilute acid treatments. The quartz fraction was purified by etching in dilute hydrofluoric and nitric acids. Prior to dissolution, the purified quartz fraction of each sample was spiked with a commercially made ^{9}Be carrier solution and dissolved in hydrofluoric acid. Procedural blanks were prepared using the same mass of the carrier added to the samples. The beryllium fraction of each sample was chemically isolated and prepared into targets for ^{10}Be/^{9}Be measurement by accelerator mass spectrometry (AMS) at the Purdue University Rare Isotope Measurement Laboratory (Muzikar et al., 2003).

Procedural blanks ^{10}Be/^{9}Be ratios range from 1.12×10^{-14} to 2.20×10^{-14} ($n=8$) and sample ^{10}Be/^{9}Be values range from 2.50×10^{-13} to 4.60×10^{-13}; therefore, for all samples, >90% of measured ^{10}Be is from *in situ* production in quartz (for most samples, blank corrections were 5% or less). One-sigma AMS uncertainties range from 2–9%, although for most samples this error is 2–4%. Surface-exposure ages for each sample were computed using the CRONUS-Earth online exposure age calculator version 2.2 (Balco et al., 2008; http://hess.ess.washington.edu/math/), based on a global reference (i.e., sea level and high latitude) production rate for *in situ* ^{10}Be and a constant production scaling scheme from Stone (2000) and Lal (1991). Surface-exposure ages were also computed using the same method of calculation but based on a lower reference production rate, calibrated for independently dated surfaces in northeastern North America (Balco et al., 2009). This production rate is similar to other recently published calibrated production rates and yields exposure ages that are ~12% older than those computed using the global reference production rate (Table 1). These regionally calibrated production rates will likely result in future refinements to the global ^{10}Be reference production rate (e.g., Lifton, 2011). Nonetheless, we report surface-exposure ages here using the current global reference production rate for the purpose of comparison with cosmogenic surface-exposure ages from elsewhere in the Great Basin, nearly all of which have been computed in the same way (e.g., Laabs et al., 2011; Rood et al., 2011).

Two major concerns when calculating surface-exposure ages for moraine boulders are the twin criteria that (1) boulder surfaces have been continuously exposed to the atmosphere since the moraine crest was abandoned, and (2) measured ^{10}Be concentrations for each sample only reflect post-depositional exposure at the moraine crest and not a prior interval of exposure. The validity of these assumptions can be evaluated by calculating a reduced chi-squared statistic (χ^2R) from the distribution of surface-exposure ages for each moraine, essentially testing whether the measurement errors (or the "internal error" in Table 1) alone can explain the observed scatter of the ages. If the χ^2R is greater than 1, which is observed frequently for Pleistocene moraines at middle latitudes (Applegate et al., 2012), then a traditional interpretation is that geologic processes account for some of the scatter (cf., Schaefer et al., 2009; Rood et al., 2011). A common geologic process is degradation of the moraine crest, which exhumes boulders that were originally shielded to cosmic rays, yielding surface-exposure ages that are younger than the true age of the moraine (Applegate et al., 2012). Numerical models of moraine-crest degradation and cosmogenic nuclide accumulation suggest that widely scattered surface-exposure ages on moraines most likely results from degradation, especially for moraines with high relief (Putkonen and Swanson, 2003). Although the low relief (~2–10 m) of all the moraines representing the Angel Lake Glaciation in Seitz Canyon suggests minimal lowering of the moraine crest (Putkonen and Swanson, 2003), boulder exhumation after moraine deposition may have contributed to the scatter of surface-exposure ages.

Given the short length (~8 km) of the glacier that occupied Seitz Canyon, the presence of inherited ^{10}Be nuclides in some boulders atop moraine crests cannot be disregarded. A small distance of glacial transport of boulders may result in insufficient removal of the ^{10}Be nuclide inventory that accumulated during a prior interval of exposure. If the sampled boulders contained a significant concentration of ^{10}Be when first deposited, then their surface-exposure ages would be older than the true age of the moraine. The potential influence of both moraine crest degradation and inherited ^{10}Be nuclides, which is not unique to Seitz Canyon, complicates identification of outliers and calculation of accurate estimates of moraine age in cases where $\chi^2R>1$.

To resolve this dilemma, a Bayesian statistical analysis was applied to surface-exposure ages of all the Angel Lake-equivalent moraines. The application of Bayesian statistics to chronological problems (described in detail by Buck et al., 1996) is a useful means of accounting for all information pertaining to a series of numerical ages. For example, consider a hypothetical stratigraphic setting in which adjacent strata have overlapping numerical age estimates. The upper layer cannot be older than the lower layer (as long as the assumption of superposition is valid); in other words, their true ages do not overlap. In Bayesian statistics, this stratigraphic observation is an example of prior information that can be used to calculate the conditional probability of an event. In geochronology, known stratigraphic relationships of a series of samples is an example of prior information that can be used to reduce the independent uncertainty of numerical age estimates of each sample yielded by, for example, propagation of counting statistics or accounting of systematic errors.

Bayesian statistical methods have been used to improve the precision of overlapping age estimates of rock and sediment layers with indisputable relative age relationships (e.g., Buck et al., 1996; Rhodes et al., 2003; Muzikar and Granger, 2006). In Seitz Canyon, our analysis takes advantage of the basic morphostratigraphic relationships between moraines; moraines are progressively younger with distance upvalley. Therefore, a Bayesian statistical analysis is applied by considering the error-weighted mean surface-exposure age ($\pm2\sigma$, weighted by the internal error) of the terminal moraine and six recessional moraines. In cases where the mean or error-weighted mean surface-exposure age violates the morphostratigraphic relationship of moraines, the analysis yields a stratigraphically consistent age of moraine crests. Additionally, in cases where the error-weighted mean surface-exposure ages of adjacent moraines overlap, the analysis yields more precise ages of each moraine. Computation of age estimates and uncertainty in this analysis is based on a Monte Carlo implementation of Bayesian statistics (Ludwig, 2003). This approach is similar to those taken by Young et al. (2011) and Stroeven et al. (2011), in that it takes advantage of sampling multiple glacial features to obtain more precise age limits on events, specifically moraine abandonment, of the last Pleistocene glaciation.

4. Results

4.1. Surface-exposure ages

Twenty-nine surface-exposure ages spanning seven moraines of the Angel Lake Glaciation provide useful numerical ages of moraines in Seitz Canyon (Table 1). Individual surface-exposure ages of moraine boulders range from 23.7 ± 2.0 ka to 13.7 ± 0.8 ka. Error-weighted mean surface-exposure ages range from 20.6 ± 0.8 ka to 15.3 ± 2.2 ka.

For seven moraine crests, χ^2R values range from 1.53 for recessional moraine 4 to 7.02 for recessional moraine 3, showing no relationship between χ^2R and the relative ages of moraines. The χ^2R values reported in Table 1 indicate that, in all cases,

the scatter of surface-exposure ages cannot be solely explained by the "internal error" of the ages (which is determined largely by the AMS measurement error; Table 1). Furthermore, the error-weighted means of surface-exposure ages from individual moraines overlap among the outer three (terminal and recessionals 1 and 2) and inner four (recessionals 3–6) moraines (Table 1, Fig. 3), and the oldest error-weighted mean surface-exposure age comes from the innermost of the three outer moraines (recessional 2). These overlapping results indicate that some combination of inherited nuclides and post-depositional modification of the moraine crest has likely affected the distribution of surface-exposure ages.

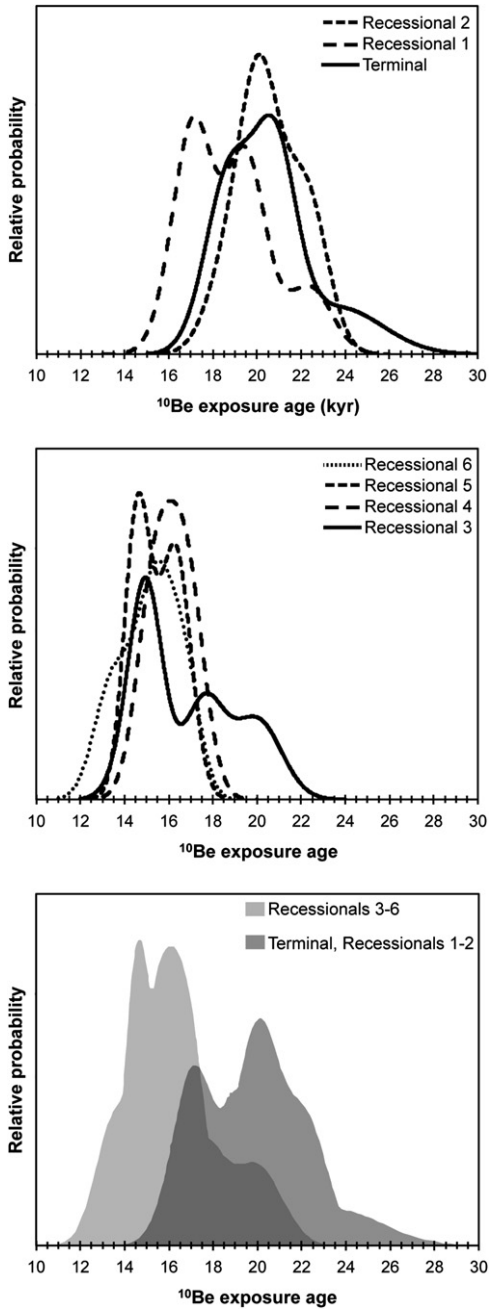

Fig. 3. Cumulative probability distribution curves of surface-exposure ages of all moraines deposited in Seitz Canyon during the Angel Lake Glaciation, computed from surface-exposure ages ($\pm 1\sigma$ internal error) from each moraine (see Fig. 2 for moraine locations). Curves computed from surface-exposure ages of the terminal, recessional 1, and recessional 2 moraines show significant overlap, as do curves computed from surface-exposure ages of recessionals 3–6. These two groupings are shown in the upper and middle panels. The area beneath the cumulative probability distribution curves of these two groupings is shaded in the lower panel. Note that the darkest area indicates where these areas overlap.

4.2. Bayesian statistics and surface-exposure ages

Applying a Bayesian statistical analysis to the assigned error-weighted means of surface-exposure ages of each of the six Angel Lake-equivalent moraines yields stratigraphically consistent surface-exposure ages of each moraine (Table 2). Because the modal surface-exposure age is the best age yielded by the Monte Carlo trials (Ludwig, 2003), it is reported for each moraine ($\pm$95% confidence; labeled the "Bayesian age" in Table 2). The uncertainty of these recalculated ages is still relatively high for moraines where the scatter of exposure ages yields high χ^2R values (e.g., Recessional 3, where χ^2R=7.02 and the 95% confidence limits are $\pm$2300/1400 yr), reflecting the potentially large systematic error of some surface-exposure ages due to inherited nuclides or boulder exhumation. Nonetheless, the Bayesian ages are considerably more precise at the 95% confidence level than moraine ages estimated from the mean or the error-weighted mean of the exposure ages (Tables 1 and 2). The Bayesian ages also provide a minimum limit on the duration of ice occupation of moraines with overlapping surface-exposure ages. For example, the terminal, recessional 1 and recessional 2 moraines have broadly overlapping Bayesian ages of 20.5 $\pm$ (0.7/0.6 ka), 20.1 $\pm$ (0.7/0.6 ka) and 20.0 $\pm$ (0.7/0.6 ka) (Table 2). A logical interpretation of these ages is that shortly after the terminal moraine was abandoned, the glacier margin rapidly retreated, and then constructed recessional moraines 1 and 2 before retreating again. Recessional moraines 3–6 were deposited somewhat later, with moraine abandonment at 17.2 $\pm$ (2.3/1.4) ka, 16.0 $\pm$ (1.0/0.7) ka, 15.3 $\pm$ ka and 14.8 $\pm$ (0.8/2.1) ka.

5. Discussion

5.1. The chronology of the Angel Lake glaciation in Seitz Canyon

The surface-exposure ages reported here indicate that the Angel Lake-equivalent moraines were deposited during marine oxygen-isotope stage 2, similar to nearly all dated terminal moraines of the last Pleistocene glaciation in the western US. Additionally, the surface-exposure ages validate correlation of the Angel Lake Glaciation to the last Pleistocene glaciation in bordering physiographic provinces: the Pinedale Glaciation in the Rocky Mountains and the Tioga Glaciation in the Sierra Nevada (Richmond and Fullerton, 1986; Fig. 4). The timing of glacier growth and initial occupation of the terminal moraine during the Angel Lake Glaciation cannot be limited by the surface-exposure ages reported here, but appears to have coincided with at least part of the global Last Glacial Maximum (LGM; 26.5–19.0 ka; Clark et al., 2009; Fig. 4). The abandonment of the terminal moraine and subsequent deposition and abandonment of recessional moraines 1 and 2 during the interval ca. 20.5 $\pm$ (0.7/0.6) ka to 20.0 $\pm$ (0.6/0.7) ka occurred during the later part of the global LGM. These observations are broadly consistent with numerous other mountain glacier settings in the western US, where terminal moraines were constructed during the early part of this time interval in the eastern Sierra Nevada in California (Phillips et al., 2009), the Wind River Mountains of western Wyoming (Gosse et al., 1995) and the central Colorado Plateau in southern Utah (Marchetti et al., 2005). In contrast, terminal moraines were abandoned much later, ca. 17 ka, in the Wallowa Mountains in eastern Oregon (Licciardi et al., 2004), the southwestern sector of the Uinta Mountains in northern Utah (Laabs et al., 2009) and numerous locales in the Middle Rocky Mountains in Colorado (Benson et al., 2005).

Table 2
Results of Bayesian analysis of error-weighted mean surface-exposure ages of moraines deposited during the Angel Lake Glaciation.

Moraine[a]	Error-weighted mean age (ka)	2σ or 95% conf.[b] (kyr)	Bayesian age[c] (ka)	+ 95% conf. (kyr)	−95% conf. (kyr)	Age difference next youngest (kyr)	+ 95% conf. (kyr)	−95% conf. (kyr)
Recessional 6	15.3	2.2	**14.8**	**0.8**	**2.1**	–	–	–
Recessional 5	15.3	0.9	**15.3**	**0.8**	**0.8**	0.1	2.5	0.08
Recessional 4	16.1	1.1	**16.0**	**1.0**	**0.7**	0.5	1.5	0.5
Recessional 3	16.3	3.5	**17.2**	**2.3**	**1.4**	0.6	2.9	0.6
Recessional 2	20.6	0.8	**20.0**	**0.6**	**0.7**	2.2	1.9	1.9
Recessional 1	18.5	1.8	**20.1**	**0.7**	**0.6**	0.04	0.7	0.03
Terminal	20.1	0.9	**20.5**	**0.7**	**0.6**	0.04	1.1	0.03

[a] See Fig. 1 for moraine locations.
[b] For recessional 1, 3 and 6, the broader 95% confidence interval is reported because the 2σ range likely underrepresents the observed variability.
[c] The modal surface exposure age computed from the distribution of the Monte Carlo trials (Ludwig, 2003) is reported here.

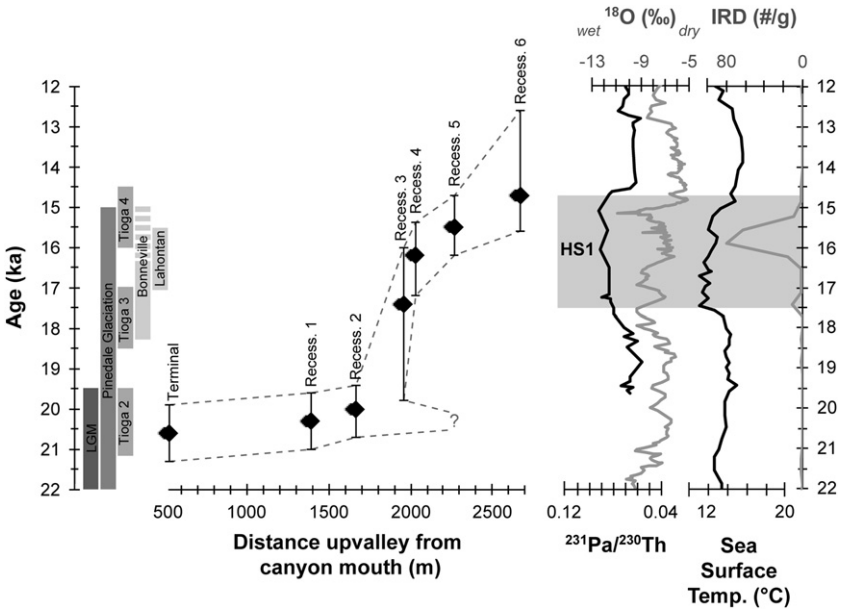

Fig. 4. Time–distance diagram of ice margin positions during the Angel Lake Glaciation in Seitz Canyon compared to regional and global records of climate change during the Latest Pleistocene. Moraine ages are the Bayesian ages (mode ± 95% confidence) given in Table 2. Gray bars indicate the timing of the latter part of the global Last Glacial Maximum (LGM; > 22.0–19.0 ka; Clark et al., 2009), the latter part of the Pinedale Glaciation (> 22.0–15.0 ka; Gosse et al., 1995; Benson et al., 2005; Ward et al., 2009), substages of the Tioga Glaciation (Tioga 2 = 21–19 ka; Tioga 3 = 18.5–17 ka; Tioga 4 = 16.0–14.5 ka; Phillips et al., 2009), the time interval when Lake Bonneville overflowed (18.3–16.4 ka, or possibly as late as 15 ka; McGee et al., 2012; Benson et al., 2011; Godsey et al., 2011), and the time when Lake Lahontan was rising to and then occupying its highest shoreline (17.0–15.5 ka; Benson et al., in press; Adams and Wesnousky, 1998). The oxygen-isotope ($\delta^{18}O$) record from Fort Stanton Cave, New Mexico (Asmerom et al., 2010; gray line), indicates relative changes in precipitation in the southwestern US. The $^{231}Pa/^{230}Th$ record from marine sediments in the subtropical Atlantic Ocean is a proxy for Atlantic meridional overturning circulation (McManus et al., 2004; black line), such that higher ratios indicate a lesser rate of overturning. The records of ice-rafted debris (IRD, black line) and sea-surface temperature (gray line) from marine sediment core SU8118 from the northeastern Atlantic Ocean (Bard et al., 2000) reflect of the interval of Heinrich Stadial 1 (HS1, light gray bar, Hemming, 2004). The inferred relationship between climate in the North Atlantic during HS1 and climate in the southwestern US (Asmerom et al., 2010) is described in the text.

The Bayesian ages of recessional moraines 2 and 3 differ in age by 2200 ± (1900/1900) kyr (Table 2; Fig. 4). Given the broad uncertainty of this age difference, it is impossible to infer whether ice retreated a significant distance up-valley after abandoning recessional 2 and then readvanced to deposit recessional moraine 3, or if it remained near its maximum extent before depositing recessional moraine 3. In either case, the broad overlap of the Bayesian ages of recessional moraines 3–6 indicates that ice was within 1.5–2 km of its maximum extent (and at least 75% of its maximum length) from just prior to 17.2 ± (2.3/1.4) until 14.8 ± (0.8/2.1) ka (Fig. 4). Mountain glaciers were at or near their latest Pleistocene extent at this time in numerous other settings in the western US, including the southeastern Sierra Nevada (Phillips et al., 2009; Rood et al., 2011), the Wallowa Mountains (Licciardi et al., 2004), the western Wasatch and Uinta Mountains (Laabs et al., 2009, 2011), the Yellowstone Plateau and adjacent mountains in northwestern Wyoming and southwestern Montana (Licciardi et al., 2001; Licciardi and Pierce, 2008), and some drainages in the Southern Rocky Mountains in Colorado (Young et al., 2011).

If the glacier in Seitz Canyon did not retreat a significant distance up valley after deposition of recessional moraine 2 but, instead paused to deposit recessional moraines 3–6, then the duration of the Angel Lake Glaciation can be limited by the Bayesian ages in Table 2. The maximum of this event began at an unknown time prior to 20.5 ± (0.7/0.6) ka and continued until 14.8 ± (0.8/2.1) ka, ending with abandonment of recessional moraine 6. Therefore, the duration of the Angel Lake Glaciation may have been greater than 6 kyr, spanning at least the later part of the global Last Glacial Maximum and the early part of last glacial–interglacial transition. The onset of final ice retreat at ca. 15 ka has been broadly observed in moraine records of western North

America (e.g., Young et al., 2011) and coincides with the end of the Heinrich Stadial 1 (Hemming, 2004) and the onset of the Bølling/Allerød warming interval of the North Atlantic region (Stanford et al., 2006).

5.2. The Angel Lake glaciation in a regional context

Models of the last Pleistocene glaciation in the western (Sierra Nevada) and eastern (Middle Rocky Mountains) extremes of the Great Basin differ in that the Tioga Glaciation of the Sierra Nevada has been subdivided into four substages, Tioga 1–4. In contrast, the Pinedale Glaciation has been only locally subdivided, and the timing of this event is observed to have varied spatially (e.g., Thackray, 2008). Below, the chronology of glacial deposits in Seitz Canyon is compared to previously reported glacial chronologies from elsewhere in the Great Basin and the Rocky Mountains. For consistency, all previously reported cosmogenic ^{10}Be surface-exposure ages discussed below have been recalculated based on the reference production rate and scaling used here.

When compared with chronologies of the Pinedale Glaciation throughout the Rocky Mountains, deposition of (and subsequent retreat from) moraines in Seitz Canyon occurred at about the same time as moraine deposition and subsequent retreat in the Wind River Mountains, where suites of moraines have been dated to ca. 23–16 ka in multiple valleys with cosmogenic ^{10}Be and ^{36}Cl (Gosse et al., 1995; Phillips et al., 1997). However, cosmogenic ^{10}Be surface-exposure ages of terminal moraines in the western Uinta and Wasatch Mountains (Laabs et al., 2009, 2011) and in some ranges in Colorado (Benson et al., 2005; Ward et al., 2009) are younger than the terminal moraine in Seitz Canyon. These apparent age discrepancies may be attributed to differences in moraine preservation or local effects on ice dynamics in these areas (e.g. Young et al., 2011), such that moraines from earlier substages of the Pinedale Glaciation were overrun by later advances. Additionally, the effects of local moisture sources on ice extent during the Latest Pleistocene may have been significant in mountain ranges immediately downwind of Pleistocene Lake Bonneville (e.g., Munroe et al., 2006). Overall though, it appears that glaciers in these regions were advancing and retreating at the same times and responding to the same regional-scale climate changes during the Latest Pleistocene. This apparent synchrony is largely independent of forthcoming, systematic refinements of the global reference production rate and scaling of *in situ* ^{10}Be (e.g., Lifton, 2011) because much of the glacial chronology of the western US is based on cosmogenic ^{10}Be surface-exposure dating.

A more specific comparison between the Angel Lake and Tioga Glaciations is possible due to the completeness of glacial chronologies at Seitz Canyon and the Bishop Creek valley in the eastern Sierra Nevada, where cosmogenic ^{36}Cl surface-exposure dating has been applied to multiple moraine crests. Deposition of the terminal and recessional 1 and 2 moraines in Seitz Canyon (at $20.5 \pm (0.7/0.6)$ ka, $20.1 \pm (0.7/0.6)$ ka and $20.0 \pm (0.6/0.7)$ ka) coincides with the Tioga 2 substage in the Sierra Nevada (21–19 ka; Phillips et al., 2009) (Fig. 4). Whether the glacier in Seitz Canyon was near its maximum extent during the time of the older Tioga 1 substage (28–24 ka; Phillips et al., 2009) is unknown; if so, the glacier in Seitz Canyon may have overrun a moraine deposited during this interval while advancing to its maximum position (note that surface-exposure ages computed with a lower reference production rate of ^{10}Be are still younger than the interval of Tioga 1) (Table 1). Because of the relatively great uncertainty of its surface-exposure age, recessional moraine 3 in Seitz Canyon ($17.2 \pm (2.3/1.4)$ ka) may correspond to either the Tioga 2 or 3 substage in the Sierra Nevada (18.5–17 ka; Phillips et al., 2009). Recessional moraines 4–6 ($16.0 \pm (1.0/0.7)$ka, $15.3 \pm (0.8/0.8)$ ka and $14.8 \pm (0.8/2.1)$ ka) match the Tioga 4 substage (16.0–14.5 ka; Phillips et al., 2009), suggesting that the onset of final ice retreat occurred nearly synchronously in Seitz Canyon and in Bishop Creek valley (Fig. 4). It should be noted, however, that the if forthcoming refinements to the production rates and scaling of *in situ* ^{36}Cl and ^{10}Be are not parallel, this comparison of the Angel Lake and Tioga Glaciations may be subject to revision.

Because of the differing sensitivities of glaciers and lakes to temperature and precipitation changes, the relative timing of mountain glaciation and highstands of Pleistocene lakes can provide clues to the nature of climate change during the Angel Lake Glaciation. The hydrologic maximum of Lake Bonneville spans the interval 18.3–15.0 ka (Benson et al., 2011), although it may have ceased overflowing as early as ca. 16.4 ka (McGee et al., 2012). Lake Lahontan was near its maximum elevation ca. 17.0–15.5 ka (Benson et al., in press; Adams and Wesnousky, 1998). These intervals of high lake levels in the Great Basin correspond to surface-exposure ages of recessional moraines 3–6 in Seitz Canyon (Table 2, Fig. 4), indicating that this glacier was still near its maximum extent during lake highstands. Synchronous maxima of mountain glaciers and pluvial lakes is also observed in the eastern Great Basin and consistent with the hypothesis that, after the global LGM, mountain glaciers were responding to the same regional-scale climate changes as the largest paleolakes (Laabs et al., 2011). This relationship holds true even if a lower reference production rate is used to compute the cosmogenic ^{10}Be surface-exposure ages presented here. The resulting age increase of 12% (Table 1) still yields overlap between the latter part of the Angel Lake Glaciation and Pleistocene lake maxima.

Synchrony of glacier and lake maxima at ca. 17–15 ka suggests that climate during this interval differed from earlier intervals of the Angel Lake, Pinedale and Tioga Glaciations, ca. 22–19 ka, when glaciers were at their maximum extents but lakes were below their highstand levels (Benson et al., in press; Oviatt, 1997). Given that lakes are more sensitive to precipitation and glaciers (in continental interior locations such as the Great Basin) to temperature, it is likely that cool and wet conditions – favoring maxima of both glaciers and lakes – persisted at ca. 17–15 ka, as opposed to cold and dry climate that has been characterized for much of the western US during the LGM (e.g., Bartlein et al., 1998). The interval 17–15 ka overlaps with Heinrich Stadial 1 (ca. 17.5–14.7 ka; Hemming, 2004), which featured large discharges of icebergs into the North Atlantic Ocean (Fig. 4). Stable isotope signatures recorded in speleothems in the southwestern US indicate cool and wet climate during this interval (Fig. 4), which may be attributed to a southward shift in the polar jet and associated storm tracks in response to cooling at northern high latitudes (e.g., Asmerom et al., 2010). Responses of Pleistocene lakes in the Great Basin to climate changes during Heinrich Stadial 1 have been identified in previous studies (e.g., Broecker et al., 2009; Munroe and Laabs, in press). As noted above, synchronous moraine deposition in the western US may reflect advance (or cessation of retreat) of small mountain glaciers in response to the same climate changes that affected lakes.

6. Conclusions

The timing of the Angel Lake Glaciation is limited by surface-exposure dating of moraines in Seitz Canyon, one of the best-preserved moraine sequences in the Great Basin. The potential geologic errors of this dating method are significantly reduced by sampling seven moraine crests with key relative age relationships and the application of a Bayesian statistical analysis that incorporates this morphostratigraphic control. This method is particularly advantageous for moraines where the potential effects of inherited nuclides and moraine-crest degradation are unknown and where surface-exposure ages from a suite of moraines

overlap as a likely result of these effects. Therefore, this approach to developing a glacial chronology from numerical age limits of moraines has potential for widespread application in settings where multiple moraines are preserved.

The glacial chronology reported here shows broad synchrony and similarity in duration between the Angel Lake Glaciation and the Tioga and Pinedale Glaciations of the Sierra Nevada and Rocky Mountains, respectively. Nonetheless, the glacial chronology of Seitz Canyon, while based on one of the best-preserved moraine suites in the interior Great Basin, may not reflect the timing of glaciation in every mountain range in this region. The Ruby Mountains are one of many glaciated ranges in the region; others at different latitudes or in closer proximity to large Pleistocene lakes may have experienced glacier maxima and subsequent retreat at different times compared to Seitz Canyon. Additional application of numerical dating methods to the glacial record elsewhere in the Great Basin will be useful for (1) improving age limits on the Angel Lake Glaciation, (2) revealing whether the timing of this event varied spatially throughout the Great Basin, and (3) providing the framework for understanding Latest-Pleistocene climate change in this extensive and under-studied region of the western US.

Acknowledgments

The authors thank the following people for their assistance with this research: M. Badding, C. Krueger, A. Leggett, K. Scalise and L. Wendler at SUNY Geneseo, and M. Bigl at Middlebury College. The authors also thank J. Licciardi and N. Young for helpful comments on an earlier version of this paper. Research was supported by a Geological Society of America Gladys W. Cole Memorial Award and NSF-EAR-0902472 to B. Laabs, and NSF-EAR-0902586 to J. Munroe. Access to the study area was granted by T. Hebert and permission to collect samples was provided by the Humboldt-Toiyabe National Forest.

References

Applegate, P.J., Urban, N.M., Keller, K., Lowell, T.V., Kelly, M.A., Laabs, B.J.C., Alley, R.B., 2012. What can we learn from the distributions of cosmogenic-exposure dates on moraines? Quat. Res. 77, 293–304.

Adams, K.D., Wesnousky, S.G., 1998. Shoreline processes and the age of the Lake Lahontan highstand in the Jessup embayment, Nevada. Geol. Soc. Am. Bull. 10, 1318–1332.

Asmerom, Y., Polyak, V.J., Burns, S.J., 2010. Variable winter moisture in the southwestern United States linked to rapid glacial climate shifts. Nat. Geosci. 3, 114–117.

Balco, G., Stone, J., Lifton, N., Dunai, T., 2008. A complete and easily accessible means of calculating surface exposure ages or erosion rates from ^{10}Be and ^{26}Al measurements. Quat. Geochronol. 3, 174–195.

Balco, G., Briner, J., Finkel, R.C., Rayburn, J.A., Ridge, J.C., Schaefer, J.M., 2009. Regional beryllium-10 production rate calibration for northeastern North America. Quat. Geochronol. 4, 93–107.

Bard, E., Rostek, F., Turon, J., Gendreau, S., 2000. Hydrological impact of Heinrich events in the subtropical Northeast Atlantic. Science 289, 1321–1324.

Bartlein, P.J., Anderson, K.H., Anderson, P.M., Edwards, M.E., Mock, C.J., Thompson, R.S., Webb, R.S., Webb III, T., Whitlock, C., 1998. Paleoclimate simulations for North America over the past 21,000 years: features of the simulated climate and comparisons with paleoenvironmental data. Quat. Sci. Rev. 17, 549–585.

Benson, L.V., Smoot, J.P., Lund, S.P., Mensing, S.A., Foit Jr., F.F., Rye, R.O. Insights from a synthesis of old and new climate-proxy data from the Pyramid and Winnemucca lake basins for the period 48 to 11.5 cal ka. Quaternary International, http://dx.doi.org/10.1016/j.quaint.2012.02.040, in press.

Benson, L.V., Lund, S.P., Smoot, J.P., Rhode, D.E., Spencer, R.J., Verosub, K.L., Louderback, L.A., Johnson, C.A., Rye, R.O., Negrini, R.M., 2011. The rise and fall of Lake Bonneville between 45 and 10.5 ka. Quat. Int. 235, 57–69.

Benson, L., Madole, R., Landis, G., Gosse, J., 2005. New data for late Pleistocene Pinedale alpine glaciation from southwestern Colorado. Quat. Sci. Rev. 24, 49–65.

Benson, L.V., Thompson, R.S., 1987. The physical record of lakes in the Great Basin. In: Ruddiman, W.F., Wright, H.E., Jr., eds., North American and adjacent oceans during the last deglaciation. Boulder, Colorado, Geological Society of America. The Geology of North America L, pp. 241–260.

Bierman, P.R., Caffee, M.W., Davis, P.T., Marsella, K., Pavich, M., Colgan, P., Mickelson, D., Larsen, J., 2002. Rates and timing of Earth-surface processes from in situ-produced cosmogenic Be-10. In: Grew, E.S. (ed.), Beryllium: Mineralogy, Petrology and Geochemistry. Rev. Mineral. Geochem. 50, 147–205.

Blackwelder, E., 1934. Supplementary notes on Pleistocene glaciation in The Great Basin. J. Wash. Acad. Sci. 24, 217–222.

Blackwelder, E., 1931. Pleistocene glaciation in the Sierra Nevada and Basin Ranges. Geol. Soc. Am. Bull. 42, 865–922.

Broecker, W.S., McGee, D., Adams, K.D., Cheng, H., Edwards, R.L., Oviatt, C.G., Quade, J., 2009. A Great Basin-wide dry episode during the first half of the Mystery Interval? Quat. Sci. Rev. 28, 2557–2563.

Buck, C.E., Cavanagh, W.G., Litton, C.D., 1996. Bayesian Approach to Interpreting Archaeological Data. John Wiley, Chichester 402 pp.

Burke, R.M., Birkeland, P.W., 1979. Re-evaluation of multiparameter relative dating techniques and their application to the glacial sequence along the eastern escarpment of the Sierra Nevada, California: Quaternary Research 11, pp. 21–51.

Clark, P.U., Dyke, A.S., Shakun, J.D., Carlson, A.E., Clark, J., Wohlfarth, B., Mitrovica, J.X., Hostetler, S.W., McCabe, A.M., 2009. The last Glacial maximum. Science 325, 710–714.

Ditchburn R. G., Whitehead N. E., 1994. The separation of ^{10}Be from silicates. 3d Workshop of the South Pacific Environmental Radioactivity Association, pp. 4–7.

Gilbert, G.K., 1890. Lake Bonneville. US Geol. Surv. Monogr. 1 438 pp.

Godsey, H.S., Oviatt, C.G., Miller, D.M., Chan, M.A., 2011. Stratigraphy and chronology of offshore to nearshore deposits associated with the Provo shoreline, Pleistocene Lake Bonneville, Utah. Palaeogeogr. Palaeoclimatol. Palaeoecol. 310, 442–450.

Gosse, J.C., Klein, J., Evenson, E.B., Lawn, B., Middleton, R., 1995. Beryllium-10 dating of the duration and retreat of the last Pinedale glacial sequence. Science 268, 1329–1333.

Hemming, S.R., 2004. Heinrich events: massive late Pleistocene detritus layers of the North Atlantic and their global climate imprint. Rev. Geophys. 42, 1–43.

Howard, K. A., Kistler, R. W., Snoke, A. W., Willden, R., 1979, Geologic map of the Ruby Mountains, Nevada, US Geological Survey Miscellaneous Geological Investigations Map I-1,136, scale 1:125,000.

Kohl, C.P., Nishiizumi, K., 1992. Chemical isolation of quartz for measurement of in situ produced cosmogenic nuclides. Geochim. Cosmochim. Acta 56, 3583–3587.

Laabs, B.J.C., Marchetti, D.W., Munroe, J.S., Refsnider, K.A., Gosse, J.C., Lips, E.W., Becker, R.A., Mickelson, D.M., Singer, B.S., 2011. Chronology of latest Pleistocene mountain glaciation in the western Wasatch Mountains, Utah, USA. Quat. Res. 76, 272–284.

Laabs, B.J.C., Refsnider, K.A., Munroe, J.S., Mickelson, D.M., Applegate, P.A., Singer, B.S., Caffee, M.W., 2009. Latest Pleistocene glacial chronology of the Uinta Mountains: support for moisture-driven asynchrony of the last deglaciation. Quat. Sci. Rev. 28, 1171–1187.

Lal, D., 1991. Cosmic ray labeling of erosion surfaces: *in situ* nuclide production rates and erosion rates. Earth Planet. Sci. Lett. 104, 424–439.

Licciardi, J.M., Pierce, K.L., 2008. Cosmogenic exposure-age chronologies of Pinedale and Bull Lake glaciations in greater Yellowstone and the Teton Range, USA. Quat. Sci. Rev. 27, 814–831.

Licciardi, J.M., Clark, P.U., Brook, E.J., Elmore, D., Sharma, P., 2004. Variable responses of western US glaciers during the last deglaciation. Geology 32, 81–84.

Licciardi, J.M., Clark, P.U., Brook, E.J., Pierce, K.J., Kurz, M.D., Elmore, D., Sharma, P., 2001. Cosmogenic ^{3}He and ^{10}Be chronologies of the late Pinedale northern Yellowstone ice cap, Montana, USA. Geology 29, 1095–1098.

Lifton, N., 2011. Potential resolution of discrepancies between scaling models for in situ cosmogenic nuclide production rates. Paper 1554, International Quaternary Congress, XVIII.

Ludwig, K.R., 2003. User's manual for Isoplot 3.00, a geochronological toolkit for Microsoft Excel, 4. Berkeley Geochronology Center Special Publication 70 pp.

Madsen, D.B., Currey, D.R., 1979. Late Quaternary glacial and vegetation changes, Little Cottonwood Canyon area, Wasatch Mountains, Utah. Quat. Res. 12, 254–270.

Marchetti, D.W., Cerling, T.E., Lips, E.W., 2005. A glacial chronology for the Fish Creek drainage of Boulder Mountain, USA. Quat. Res. 64, 263–271.

McGee, D., Quade, J., Edwards, R.L., Broecker, W.S., Cheng, H., Reiners, P.W., Evenson, N., 2012. Lacustrine cave carbonates: novel archives of paleohydrologic change in the Bonneville Basin (Utah, USA). Earth Planet. Sci. Lett. 351–352, 182–194.

McManus, J.F., Francois, R., Gherardi, J.-M., Keigwin, L.D., Brown-Leger, S., 2004. Collapse and rapid resumption of Atlantic meridional circulation linked to deglacial climate changes. Nature 428, 834–837.

Munroe, J.S., Laabs, B.J.C. Temporal correspondence between pluvial lake highstands in the southwestern US and Heinrich Event 1. J. Quat. Sci, http://dx.doi.org/10.1002/jqs.2586, in press.

Munroe, J.S., Laabs, B.J.C., 2011. New investigations of Pleistocene glacial and pluvial records in northeastern Nevada. In: Evans, J.P., Lee, J. (Eds.), Geologic Field Trips to the Basin and Range, Rocky Mountains, Snake River Plain, and Terranes of the US, 21. Geological Society of America Field Guide, Cordillera, pp. 1–25.

Munroe, J.S., Laabs, B.J.C., Shakun, J.D., Singer, B.S., Mickelson, D.M., Refsnider, K.A., Caffee, M.W., 2006. Latest Pleistocene advance of alpine glaciers in the southwestern Uinta Mountains, Utah, USA. Evidence for the influence of local moisture sources. Geology 34, 841–844.

Muzikar, P., Granger, D., 2006. Combining cosmogenic, stratigraphic, and paleomagnetic information using a Bayesian approach: general results and an application to Sterkfontein. Earth Planet. Sci. Lett. 214, 400–408.
Muzikar, P., Elmore, D., Granger, D.E., 2003. Accelerator mass spectrometry in geologic research. Geol. Soc. Am. Bull. 115, 643–654.
Nishiizumi, K., Imamura, M., Caffee, M.W., Southon, J.R., Finkel, R.C., McAninch, J., 2007. Absolute calibration of 10Be AMS standards. Nucl. Instrum. Methods Phys. Res. B 258, 403–413.
Osborn, G., Bevis, K., 2001. Glaciation of the Great Basin of the western United States. Quat. Sci. Rev. 20, 1377–1410.
Oviatt, C.G., 1997. Lake Bonneville fluctuations and global climate change. Geology 25, 155–158.
Phillips, F.M., Zreda, M., Plummer, M.A., Elmore, D., Clark, D.H., 2009. Glacial geology and chronology of Bishop Creek and vicinity, eastern Sierra Nevada, California. Geol. Soc. Am. Bull. 121, 1013–1023.
Phillips, F.M., Zreda, M.G., Gosse, J.C., Klein, J., Evenson, E.B., Hall, R.D., Chadwick, O.A., Sharma, P., 1997. Cosmogenic 36Cl and 10Be ages of Quaternary glacial and fluvial deposits of the Wind River Range, Wyoming. Geol. Soc. Am. Bull. 109, 1453–1463.
Phillips, F.M., Zreda, M.G., Smith, S.S., Elmore, D., Kubik, P.W., Sharma, P., 1990. Cosmogenic chlorine-36 chronology for glacial deposits at Bloody Canyon, eastern Sierra Nevada. Science 248, 1529–1532.
Porter, S.C., Pierce, K.L., Hamilton, T.D., 1983. Late Wisconsin mountain glaciation in the western United States. In: Porter, S.C. (Ed.), Late-Quaternary Environments in the Western United States. The late Pleistocene, vol. 1. University of Minnesota Press, Minneapolis, pp. 71–111.
Putkonen, J., Swanson, T., 2003. Accuracy of cosmogenic ages for moraines. Quat. Res. 59, 255–261.
Reheis, M, 1999. Extent of Pleistocene lakes in the western Great Basin. US Geological Survey Miscellaneous Field Studies Map MF-2323.
Rhodes, E.J., Bronk Ramsey, C., Outram, C., Batt, C., Willis, L., Dockrill, S., Bond, J., 2003. Bayesian methods applied to the interpretation of multiple OSL dates: high precision sediment ages from Old Scatness Brock excavations, Shetland Isles. Quat. Sci. Rev. 22, 1231–1244.
Richmond, G.M., Fullerton, D.S., 1986. Summation of Quaternary glaciations in the United States of America. Quat. Sci. Rev. 5, 183–196.
Rood, D.H., Burbank, D.W., Finkel, R.C., 2011. Chronology of glaciations in the Sierra Nevada, California from ^{10}Be surface exposure dating. Quat. Sci. Rev. 30, 646–661.
Satarugsa, P., Johnson, R.A., 2000. Cenozoic tectonic evolution of the Ruby Mountain metamorphic core complex and adjacent valleys, northeastern Nevada, Rocky Mountain. Geology 35, 205–230.
Schaefer, J.M., Denton, G.H., Kaplan, M., Putnam, A., Finkel, R.C., Barrell, D.J.A., Andersen, B.G., Schwartz, R., Mackintosh, A., Chinn, T., Schluchter, C., 2009. High-frequency Holocene glacier fluctuations in New Zealand differ from the northern signature. Science 324 (5927), 622–625.
Sharp, R.P., 1938. Pleistocene Glaciation in the Ruby-East Humboldt Range, northeastern Nevada. J. Geomorphol. 1, 296–323.
Stanford, J.D., Rohling, E.J., Hunter, S.E., Roberts, A.P., Rasmussen, S.O., Bard, E., McManus, J., Fairbanks, R.G., 2006. Timing of meltwater pulse 1a and climate responses to meltwater injections. Paleoceanography 21 (PA4), 103.
Stone, J.O., 2000. Air pressure and cosmogenic isotope production. J. Geophys. Res. B Solid Earth Planets 105, 23,753–23,759.
Stroeven, A.P., Fabel, D., Harbor, J.M., Fink, D., Caffee, M.W., Dahlgren, T., 2011. Importance of sampling across an assemblage of glacial landforms for interpreting cosmogenic ages of deglaciation. Quat. Res. 76, 148–156.
Thackray, G.D., 2008. Varied climatic and topographic influences on Late Plesticene mountain glaciation in the western United States. J. Quat. Sci. 23, 671–681.
Ward, D.J., Anderson, R.S., Guido, Z.S., Briner, J.P., 2009. Numerical modeling of cosmogenic deglaciation records, Front Range and San Juan Mountains, Colorado. J. Geophys. Res. 114, F01026.
Young, N.E., Briner, J.P., Leonard, E.M., Licciardi, J.M., Lee, K., 2011. Assessing climatic and nonclimatic forcing of Pinedale glaciation and deglaciation in the western United States. Geology 39, 171–174.